Progress In Electromagnetics Research B, Vol. 25, 171–189, 2010

E-FIELD EXTRACTION FROM *H*-NEAR-FIELD IN TIME-DOMAIN BY USING PWS METHOD

B. Ravelo

IRSEEM — EA 4353, Engineering School ESIGELEC
Technopole de Madrillet, Avenue Galilée, BP 10024,
Saint-Etienne-du-Rouvray Cedex 76801, France

Abstract—A novel technique of the electric- or E-field extraction from the magnetic- or H-near-field in time-domain is reported. This technique is based on the use of the Maxwell-Ampere relation associated to the plane wave spectrum (PWS) transform. It is useful for the E-near-field computations and measurements which are practically complicated in time-domain in particular, for the EMC applications. The considered EM-field radiation is generated by a set of electric dipoles excited by an ultra-short duration current having frequency bandwidth of about 10-GHz. The presented EM-field calculation technique is carried out by taking into account the evanescent wave effects. In the first step, the time-dependent H-field data mapped in 2-D plan placed at the height z_0 above the radiating devices are transposed in frequency-dependent data through the fast Fourier transform. In order to respect the near-field approach, the arbitrary distance z_0 between the EM-field mapping plan and radiating source plan should be below one-sixth of the excitation signal minimal wavelength. In the second step, one applies the PWS transform to the obtained frequency-data. Then, through the Maxwell-Ampere relation, one can extract the E-field from the calculated PWS of the H-field. In the last step, the inverse fast Fourier transform of the obtained E-field gives the expected time-dependent results. The relevance of the proposed technique was confirmed by considering a set of five dipole sources placed arbitrarily in the horizontal plan equated by $z = 0$ and excited by a pulse current having amplitude of 50 mA and half-width of about 0.6 ns. As expected, by using the H_x, H_y and H_z 2-D data calculated with Matlab in the rectangular plan placed at $z_0 = 3$ mm and $z_0 = 5$ mm above the radiating source, it was demonstrated that

Received 13 July 2010, Accepted 25 August 2010, Scheduled 27 August 2010
Corresponding author: B. Ravelo (blaise.ravelo@esigelec.fr).

with the proposed technique, one can determine the three components of the E-field E_x, E_y and E_z.

1. INTRODUCTION

With the incessant increase of electrical and electronic system integration densities in high performance modern equipments such as mobile phones, notebooks, electronic handsets, electric engines and automotive vehicles, the eventual issues caused by electromagnetic interference (EMI) cannot be neglected [1–10]. In fact, EMI can generate unwanted noise currents or voltages in the electric circuits which can be a source of electronic system malfunction. To overcome these technical issues, explicit studies on these topics have been conducted by electronic engineers and researchers in the matter of electromagnetic compatibility (EMC) [5, 6]. Thus in this area, investigations on undesired EM conducting and also radiating emissions have been carried out [7–10]. In order to assess the eventual EM emissions of electronic modules for the EMI/EMC applications, a modelling technique based-on the optimized combination of dipole elements were reported in [9, 10]. In fact, the consideration of EM dipole elements offers a possibility to develop simpler analytical expressions of EM-field radiation especially in near-field. But most of the published research papers on this topic have been consecrated to EM emission analysis in frequency-domain which corresponds only to permanent radiation phenomena [1–10]. However, few investigations have been realized for transient EM-field analysis in time-domain [8, 11, 12]. Even though only the analysis in time-domain permits the achievement of reliable modelling of the transient radiation effects especially for wide frequency-bandwidth EM-fields. This kind of EM-analysis necessitates efficient theoretical approaches in particular, for the study of current high-speed electronic device radiations in near-field. Knowing that in modern complex electrical and electronic embedded systems, the effects of very short duration EM-pulse radiation remain an open question. In numerous electronic modules, the influence of the EM-radiations induced by the non-linear electronic components as the diodes and MOSFETs needs actually to be evaluated. As a practical example, the current and/or voltage commutations in the digital circuits on PCB can generate a dominant E-field radiation in near zone or at the distance less than one-sixth of the wavelength from the generator circuit. Furthermore, it is interesting to note that due to the coupling effects with the test device and electric probe implementation difficulty, the E-field measurement is very difficult at high frequencies. Whereas the measurement of

H-near field emission is easier to perform by using a magnetic loop probe. In addition, the E-field computation in time-domain is still difficult to realize with certain EM-tools as Maxwell3D [13]. In fact, this simulation tool is capable to calculate only the H-field emitted by EM structures excited by electrical sources which are analytically or numerically defined in time-domain.

To cope with this bottleneck, an accurate technique of transient E-field radiation calculation in time-domain from the given H-field is proposed in this paper. The herein introduced E-field extraction method is based-on the exploitation of the plane wave spectrum (PWS) theory. As reported in [14–17], this transformation allows the decomposition of any EM-field components mapped in 2-D plan as being the sum of 2-D harmonic spectrums of the EM-plane waves propagating in different space directions. So by using the PWS theoretical concept combined with the Maxwell-Ampere relation, one can develop a computation method allowing the extraction of the E-field from the H-field in the frequency-domain. In this optic, an E-field extraction technique from the H-field extended in time-domain is developed in this paper.

To make this paper easier to understand, it is divided in four main sections. Section 2 describes, in details, the different steps concerning the methodology and the principle of the proposed technique. The considered analytical approaches for the calculation of E-field components from the H-field ones by using the Maxwell-Ampere relation and the *fft* combined with the *PWS*-transform are developed. Section 3 describes the theoretical analysis of the elementary electric dipole in time-domain. Immediately afterward, Section 4 demonstrates the feasibility of the proposed technique through its implementation into Matlab program. Lastly, Section 5 presents the conclusion of this work.

2. METHODOLOGY OF THE PROPOSED TIME-DOMAIN *E*-FIELD CALCULATION TECHNIQUE

For starting, one assumes the magnetic field $\vec{H}(x, y, z, t)$ having three components denoted $H_x(x, y, z, t)$, $H_y(x, y, z, t)$ and $H_z(x, y, z, t)$ at the point with coordinate (x, y, z) and at time t as given data. For the sake of simplification, through this section these three components are represented by the term H_ξ with the subscript ξ belonging to $\{x, y, z\}$. In other word, ξ can be x or y or z. One supposes that the given H-field 2-D data are mapped in the horizontal plan referenced in the rectangular system $(Oxyz)$ as depicted in Fig. 1. As illustrated in this figure, the geometrical continuous parameters x and y are replaced by

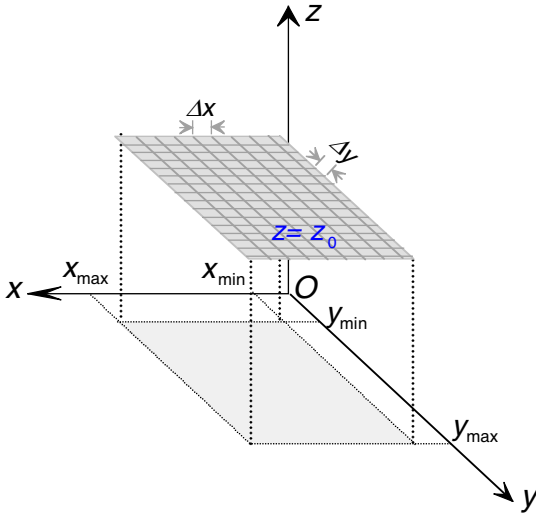

Figure 1. Description of the space-parameters for the representation of the H-field components $H_\xi(x, y, z, t)$ with $\xi = \{x, y, z\}$.

the discretized variables with the minimal and maximal limit values respectively, denoted $x_{\min}$, $x_{\max}$ and $y_{\min}$, $y_{\max}$, and with step Δx and Δy, during the numerical computations.

This magnetic field $H_\xi(x, y, z = z_0, t)$ is also defined as a time-dependent field in the function of discrete time-vector t delimited by $t_{\min}$ and $t_{\max}$, and with a step Δ_t. In near-field, the distance z_0 between the radiating source supposed placed in the (Oxy) plan equated by $z = 0$ and the mapping plan where $H_\xi(x, y, z = z_0, t)$ is given must verify the condition:

$$z_0 \leq \frac{\lambda_{\min}}{2\pi}, \tag{1}$$

with $\lambda_{\min}$ being the shortest wavelength of the considered H-field. One recalls that this wavelength is related to the bandwidth $F_{\max}$ of the considered excitation transient signal by the relation $\lambda_{\min} = v/F_{\max}$ for the wave speed v. Before the application of PWS transformation, at each point with coordinate (x, y, z), one needs to transpose this time-dependent H-field as a frequency-dependent data by using the classical *fft*:

$$H_\xi(x, y, z, f) = fft[H_\xi(x, y, z, t)]. \tag{2}$$

Then, at each frequency f, one can calculate the *PWS*-transform of

$H_\xi(x, y, z, f)$ with the following mathematical expression [14–21]:

$$P_{H_\xi}(f_x, f_y, f) = \int_{-\infty}^{\infty}\int_{-\infty}^{\infty} H_\xi(x, y, f)e^{2\pi i(f_x x+f_y y)}dxdy, \tag{3}$$

where f_x and f_y are 2-D space-frequency variables which are related to the two first components of the wave vector:

$$\vec{k} = 2\pi(f_x\vec{u}_x + f_y\vec{u}_y + f_z\vec{u}_z). \tag{4}$$

In discrete variables, these two space-frequency variables are, respectively, defined between the minimal and maximal values:

$$f_{\xi\,\min} = \frac{1}{\xi_{\max} - \xi_{\min}}, \tag{5}$$

and

$$f_{\xi\,\max} = \frac{1}{\Delta\xi}, \tag{6}$$

with step

$$\Delta f_{\xi\,\min} = \frac{1}{\xi_{\max} - \xi_{\min}}, \tag{7}$$

where the subscript ξ belongs to $\{x, y\}$. According to the PWS theory, the space-frequency variable corresponding to the z-component of the wave vector is defined as [18–21]:

$$f_z = \begin{cases} \sqrt{\frac{f^2}{v^2} - f_x^2 - f_y^2} & \text{if } f_x^2 + f_y^2 \le \frac{f^2}{v^2} \\ -i\sqrt{f_x^2 + f_y^2 - \frac{f^2}{v^2}} & \text{if } f_x^2 + f_y^2 > \frac{f^2}{v^2} \end{cases}, \tag{8}$$

where v and i represent, respectively, the wave propagation speed and the complex number $\sqrt{-1}$. It is noteworthy that for the case where $f_x^2 + f_y^2 \le f^2/v^2$, we have the propagative EM-wave because the term $e^{-i\cdot 2\pi f_z\cdot z}$ corresponds to the permanent regime. In the contrary case $f_x^2 + f_y^2 > f^2/v^2$, the term $e^{-i\cdot 2\pi f_z\cdot z}$ corresponds to a decreasing real quantity when z increases. It means that the associated EM-wave is evanescent. It is interesting to note that this extraction technique does not work in near-field domain, when the evanescent EM-waves are neglected. This constitutes the main difference with the application of Maxwell-Ampere relation in far-field where one can directly use relation (9) because the EM-fields behave generally as plane wave.

As explained in Fig. 2, with the successive *fft*- and *PWS*-operations, and the application of the Maxwell-Ampere relation, one can obtain the PWS of the associated E-field, $P_{E_\xi}(f_x, f_y, f)$ for $z = z_0$. It is well-known that according to the plane wave propagation

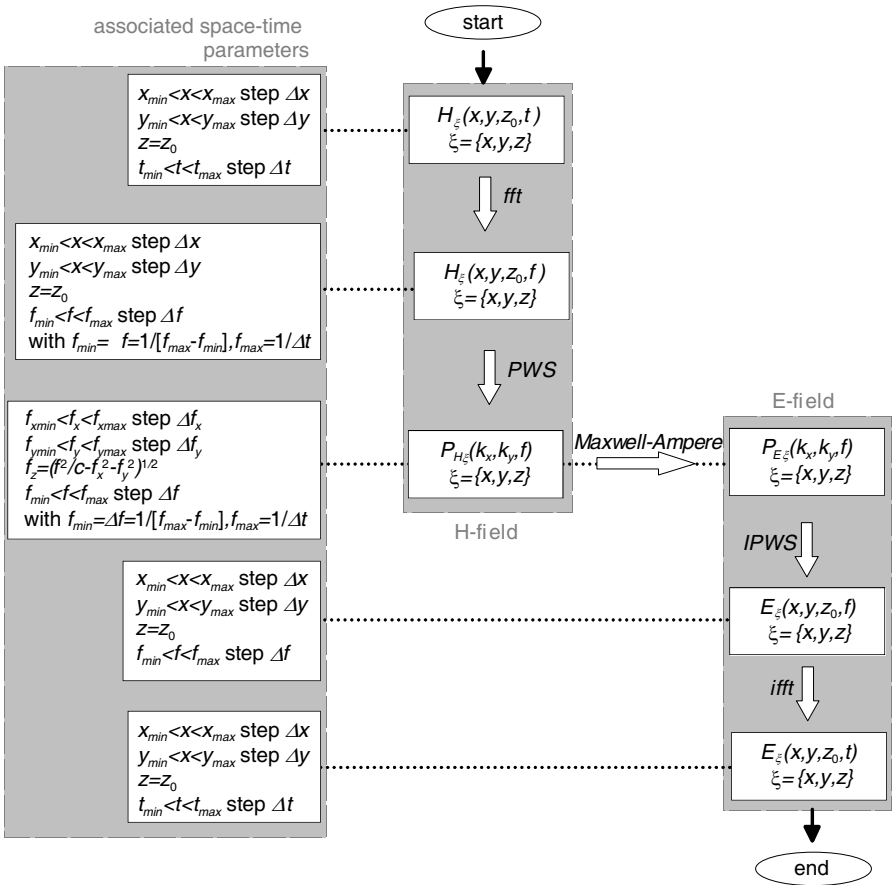

Figure 2. Flow chart summarizing the proposed E-field extraction technique from the H-near field in time-domain.

theory, when $\vec{H}$ behaves as a plane and monochromatic wave at the operating frequency f in the homogeneous and isotropic medium with relative permittivity ε_r, the E-field vector $\vec{E}$ can be extracted from the following Maxwell-Ampere relation:

$$\vec{E} = \frac{-\vec{k} \wedge \vec{H}}{2\pi f \varepsilon_r \varepsilon_0}. \tag{9}$$

Substituting $\vec{E}$ and $\vec{H}$ by their PWS terms $\vec{P}_E$ and $\vec{P}_H$ respectively, and the wave vector $\vec{k}$ by its expression introduced in (4), the previous

Maxwell-Ampere relation will be reduced as follows:

$$\begin{cases} P_{E_x} = \frac{-1}{2\pi f \varepsilon_r \varepsilon_0}(f_y P_{H_z} - f_z P_{H_y}) \\ P_{E_y} = \frac{-1}{2\pi f \varepsilon_r \varepsilon_0}(f_z P_{H_x} - f_x P_{H_z}) \\ P_{E_z} = \frac{-1}{2\pi f \varepsilon_r \varepsilon_0}(f_x P_{H_y} - f_y P_{H_x}) \end{cases}, \tag{10}$$

with $\varepsilon_r \varepsilon_0$ expressing the absolute permittivity of the considered propagation medium. Afterwards, toward the application of the equivalent inverse operations $IPWS$ and *ifft* to $P_{E_\xi}(f_x, f_y, f)$:

$$E_\xi(x, y, f) = \int_{-\infty}^{\infty} \int_{-\infty}^{\infty} P_{E_\xi}(f_x, f_y, f) e^{-2\pi i(f_x x + f_y y)} df_x df_y, \tag{11}$$

$$E_\xi(x, y, t) = ifft[E_\xi(x, y, f)], \tag{12}$$

one can extract the time-dependent E-field components $E_\xi(x, y, z = z_0, t)$ with ξ belonging to $\{x, y, z\}$.

Compared to the finite-differences time domain (FDTD) method, the under study computation method enables to realize simplified direct calculations in 2-D. More precisely, the E-field value can be assessed directly in the given mapping plan as highlighted in Fig. 1 where the H-field is already predefined. Substantially, from the time-domain measured H-field data in 2-D, one can deduce easily the associated E-field, that is not the case of the computation through FDTD method. So it is beneficial for the measurement of EM-field. It is undoubtedly advantageous in terms of the measurement and computation times. In practice (for example in EMC applications), this is particularly important for the analysis of the electronic device emissions and also for the investigation of the immunity of victim circuits neighbouring the radiating source.

3. DESCRIPTION OF THE CONSIDERED TRANSIENT RADIATION SOURCE

In order to evidence the functioning of the proposed EM-field calculation technique, let us consider the hertzian electric dipole element radiating source excited by the ultra-short duration transient pulse current $I(t)$. As reported in [22–24], the definition of the dipole moment exhibited by a time-dependent electric dipole having a physical length d at the time t on the point M situated at the distance r of this source is expressed as:

$$\vec{p}_E(r, t) = d \left[\int_0^t I(\tau) d\tau \right] \delta(r) \cdot \vec{u}, \tag{13}$$

where $\vec{u}$ represents the direction of the dipole axis. As described in [24], In the considered medium characterized by the wave speed v, the time delayed variable is defined as $t' = t - r/v$. Supposing that the source is placed at the origin of the referential system, one can define the spherical space-region delimited by the maximal radius $r_{\max}$ of the traveling wave at the time t as $r_{\max} = v \cdot t$. In 3-D space, this corresponds to the sphere equated by:

$$\sqrt{x^2 + y^2 + z^2} = v \cdot t. \tag{14}$$

In the case of propagation in the vacuum, it yields the concentric spheres with radius proportional to the time t as explained in Fig. 3. In other words, when a radiating source is placed at the centre of a coordinate system, the EM-field does not exist outside these spheres at the indicated time t.

In the 2-D horizontal plan equated by $z = z_0$ as highlighted in Fig. 1, the family of curves delimiting the zone of the radiating EM-field existence is defined as concentric circles with equation:

$$x^2 + y^2 = v^2 \cdot t^2 - z_0^2. \tag{15}$$

Equation (12) allows to define the space region limit where the EM-wave exists in the function of time t. For example, at the time $t = 1\,\text{ns}$, $\sqrt{x_{\max}^2 + y_{\max}^2}$ must be inferior to $0.3\,\text{m}$. Fig. 4 shows the circular limits where the EM-wave can be determined in the plan parallel to (Oxy) equated by $z_0 = 5\,\text{mm}$ when the radiating punctual source is placed at the origin $O(0, 0)$ for the wave speed $v = 3.10^8\,\text{m/s}$.

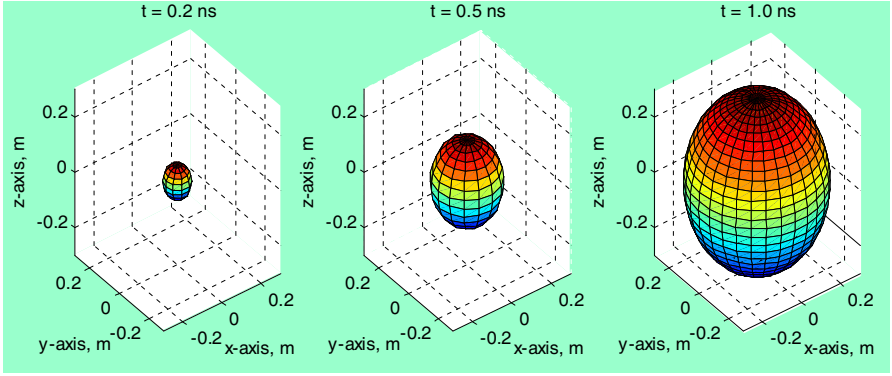

Figure 3. Space region limits (maximal distance of the source) of the propagating wave existence in the vacuum versus time by assuming a radiating source placed at $O(0, 0, 0)$.

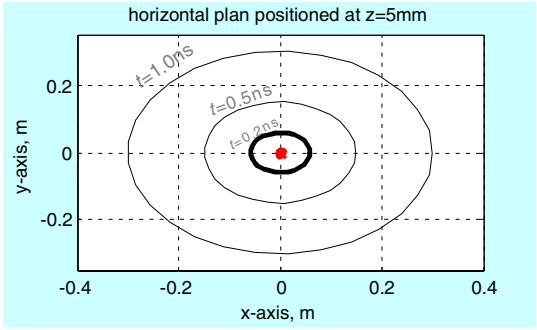

Figure 4. Circular limits of the EM-wave existence in the plan placed at $z = 5\,\text{mm}$ above the electric dipole radiating source versus time in the vacuum.

To materialize the feasibility of these theoretical concepts, let us continue with the analysis and discussion on the computed results showing the extraction of E-field knowing the H-near-field by assuming a radiating source formed by a set of electric dipoles excited by an ultra short pulse current.

4. VALIDATION RESULTS

The here presented computation results were determined in four successive steps according to the indication in the flow chart presented in Fig. 2. In the first step, as input data, the time-dependent excitation current $I(t)$ for the discrete time t varying from $t_{\min}$ to $t_{\max}$ step Δt, the physical characteristics and geometrical parameters of the considered propagation medium, and the placements of the radiating electric dipoles need to be specified. In the second step, one calculates the whole H-field components in the defined mapping plan in the function of x, y and z_0. In the next step, one applies successively the *fft* and *PWS*-transforms to the calculated H-fields. In the final step, toward the Maxwell-Ampere relation expressed in (9) yields the extraction of the E-field in frequency-domain for f varying from $f_{\min} = 1/(t_{\max} - t_{\min})$ to $f_{\max} = 1/\Delta t$ step $\Delta f = 1/(t_{\max} - t_{\min})$. Finally, through the application of the *ifft*, one gets the expected E-field data in time domain. In order to confirm the relevance of the proposed technique, these results are here compared to the E-field directly calculated from the electric dipoles.

One underlines that the computed results presented in this section were executed with the standard scientist language Matlab. Fig. 5

represents the placement of the considered set of elementary electric dipoles having a physical length $d = 0.5$ mm as a radiating source. One can see that it is composed by the combination of five dipole elements placed at the points in the plan equated by $z = 0$ with coordinates $S_1(-7\,\text{mm}, 0)$, $S_2(-3.5\,\text{mm}, 0)$, $S_3(0, 0)$, $S_4(3.5\,\text{mm}, -3.5\,\text{mm})$ and $S_5(3.5\,\text{mm}, 3.5\,\text{mm})$ which are chosen arbitrarily within the circle with 7 mm-radius. It is interesting to note that the directions of the considered dipole axis placed at the points S_1, S_3 and S_5 are oriented along (Oz); S_4 is along (Oy); and S_5 is along (Ox).

These dipoles are excited by the ultra-short duration transient current $I(t)$ which is a typically time-dependent bi-exponential pulse plotted in Fig. 6(a). This current presents a base band frequency

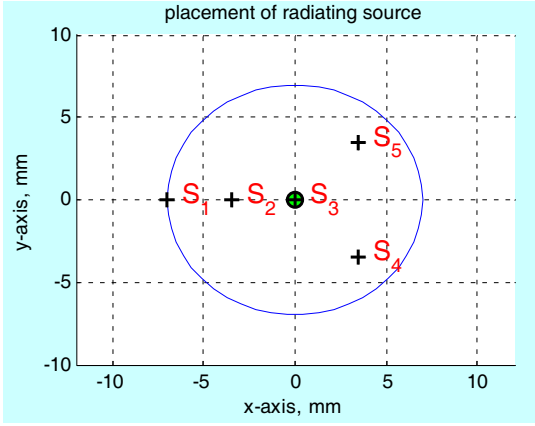

Figure 5. Under consideration radiating source.

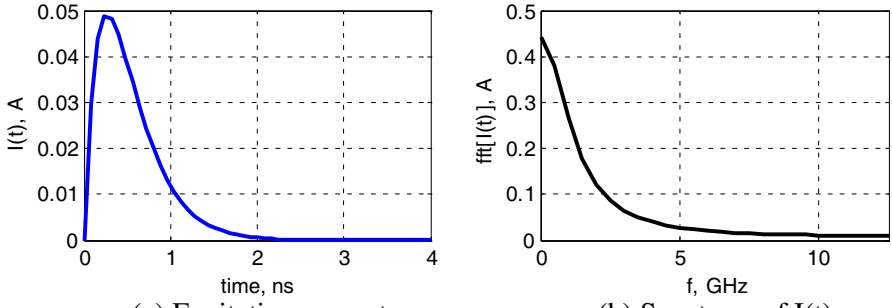

(a) Excitation current (b) Spectrum of I(t)

Figure 6. (a) Transient excitation current and (b) its frequency spectrum.

spectrum shown in Fig. 6(b). One remarks that most or 95-% of the excitation signal spectrum energy belongs to the frequency bandwidth delimited at $F_{\max} = 10\,\text{GHz}$.

Clearly, it means that by assuming that the considered medium as vacuum, the minimal wavelength of the EM-field radiated by this source is equal to $\lambda_{\min} = \frac{c}{F_{\max}} = 30\,\text{mm}$. So, according to condition (1), in order to operate in EM-near-field, one must choose the mapping plans placed at the distance $z_0 \leq \frac{\lambda_{\min}}{2\pi} \approx 5\,\text{mm}$ of the radiating source.

Regarding the above described radiation source, one determines the tensorial data corresponding to the time-dependent H-field components $H_x(x, y, z, t)$, $H_y(x, y, z, t)$ and $H_z(x, y, z, t)$ for $z = 3\,\text{mm}$ and $z = 5\,\text{mm}$ above the plan (Oxy) for t varying from $t_{\min} = 0\,\text{ns}$ to $t_{\max} = 4\,\text{ns}$ step $\Delta t = 0.08\,\text{ns}$. Therefore, one gets the results displayed in Fig. 7. This figure represents the cartographies of the calculated H-field components in the rectangular plans equated by $z = 3\,\text{mm}$

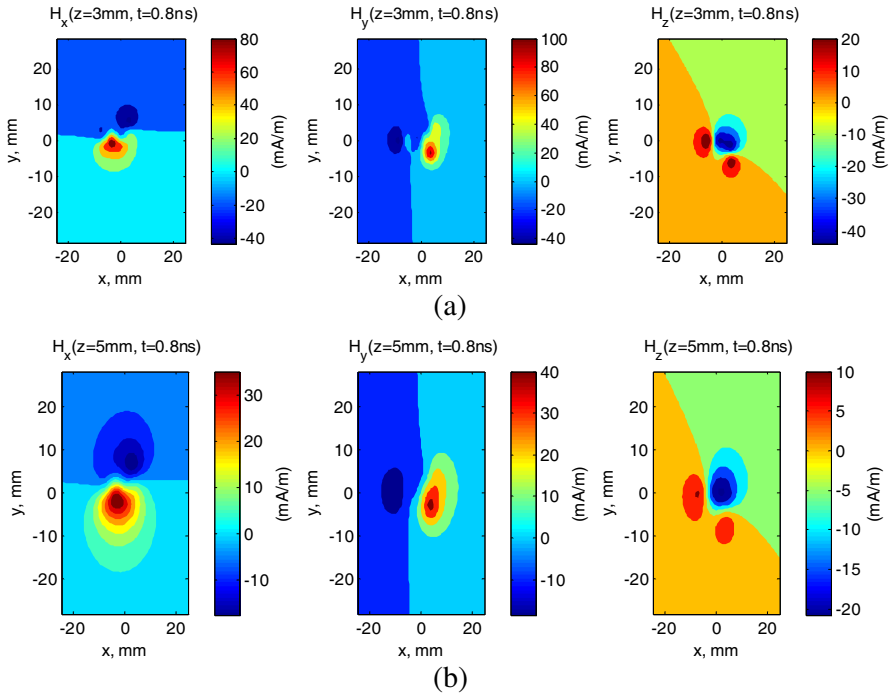

Figure 7. Cartographies of the calculated H-field components, H_x, H_y and H_z considered for extracting the E-field at (a) $z = 3\,\text{mm}$ and (b) $z = 5\,\text{mm}$, above the radiating source and at the time $t = 0.8\,\text{ns}$.

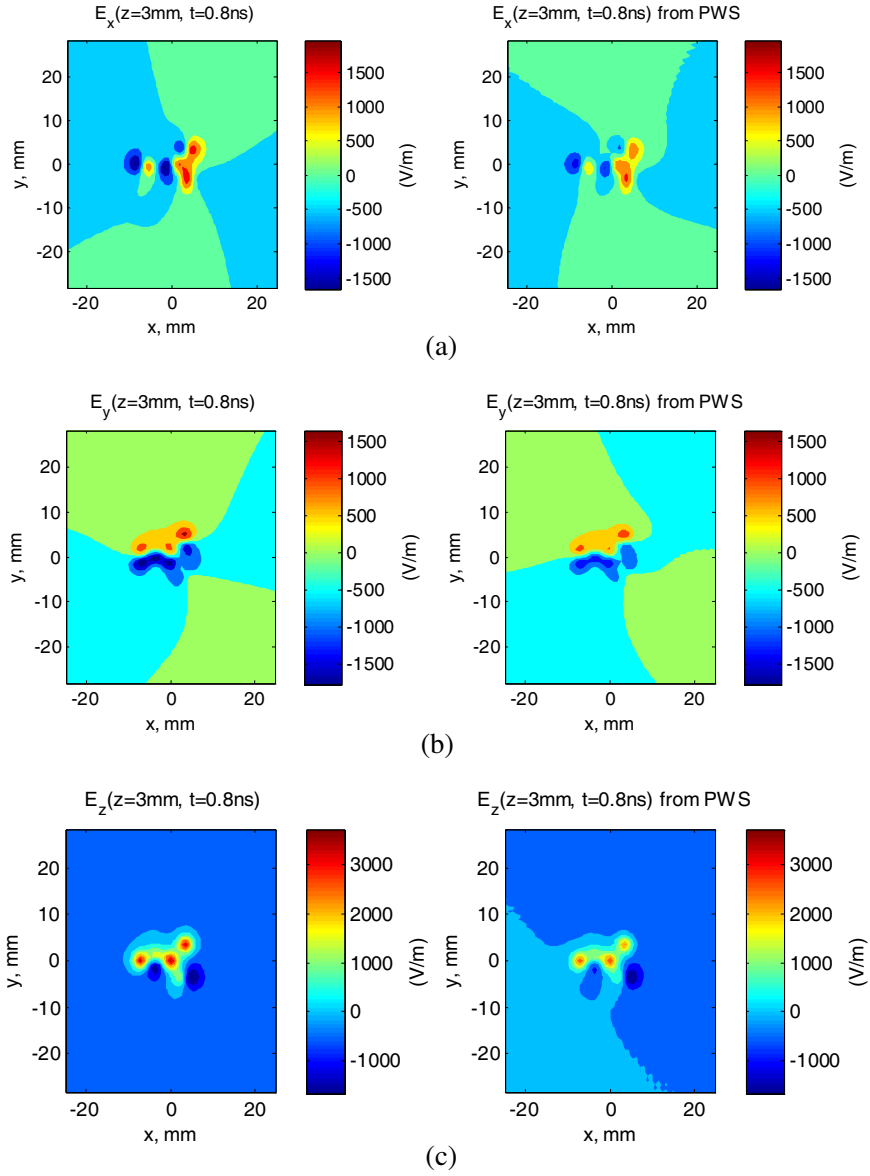

Figure 8. Comparisons of the E-field directly calculated (in left) and extracted from the proposed technique (in right) at $t = 0.8\,\text{ns}$ and $z = 3\,\text{mm}$: (a) E_x, (b) E_y and (c) E_z.

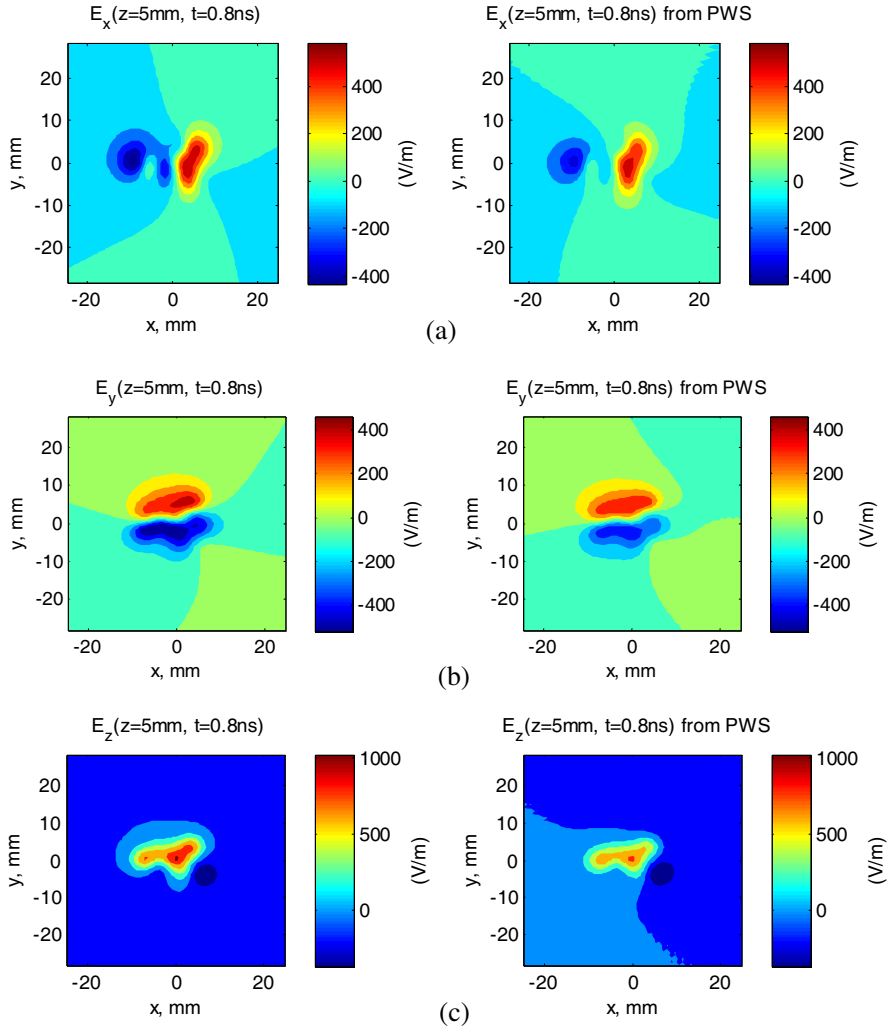

Figure 9. Comparisons of the E-field directly calculated (in left) and extracted from the proposed technique (in right) at $t = 0.8\,\text{ns}$ and $z = 5\,\text{mm}$: (a) E_x, (b) E_y and (c) E_z.

and $z = 5\,\text{mm}$ which are delimited by $x_{\max} = -x_{\min} = 25\,\text{mm}$ and $y_{\max} = -y_{\min} = 28\,\text{mm}$ with the resolution corresponding to the number of points $N_x \times N_y = 171 \times 171$ at the arbitrary chosen time $t = 0.8\,\text{ns}$.

After the implementation of the proposed calculation algorithm earlier represented by the flow chart of Fig. 2 in Section 2 into Matlab

code, one obtains the three E-field component cartographies stated in Fig. 8 for $z = 3\,\text{mm}$ and in Fig. 9 for $z = 5\,\text{mm}$. As expected, very good agreement with the cartographies of the reference exact E-field calculated directly with the considered dipoles is observed. In addition, this finding is also confirmed by the comparison between the whole E-field modulus from the analytical calculation and from the proposed PWS method Fig. 10.

One points out that due to the inaccuracy related to the space-resolutions Δx and Δy, one evaluates here relative errors below 10% for the cartographies of the three E-field components.

In order to achieve clearer and more convincing representation enabling to show the relevance of the under study calculation technique, a comparison between the profiles of E-field components from the analytical calculation and from the proposed PWS method

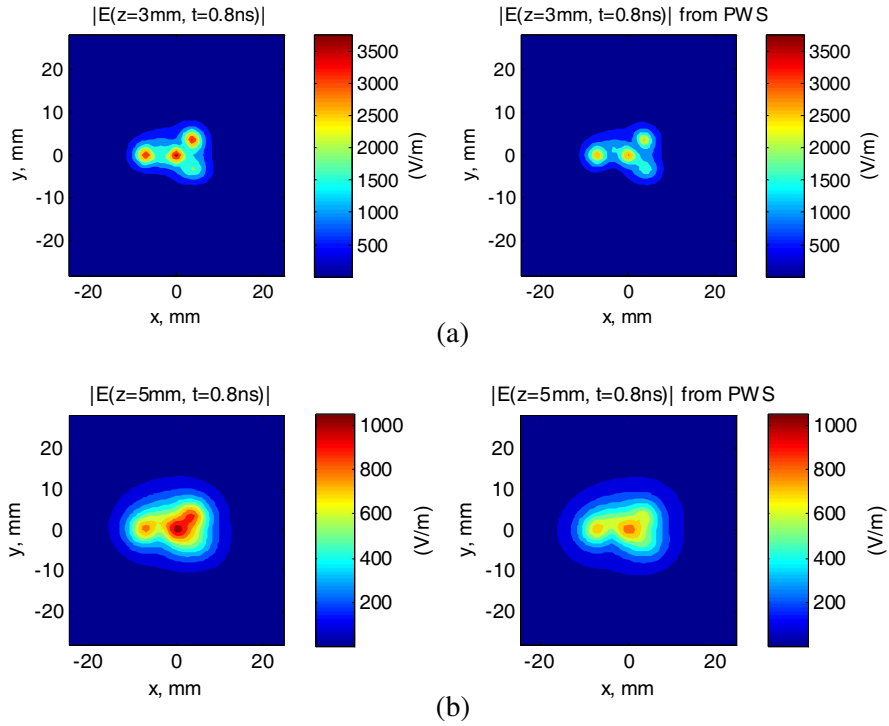

Figure 10. Modulus of the E-field directly calculated (in left) and the E-field extracted from the proposed technique (in right) at (a) $z = 3\,\text{mm}$ and (b) $z = 5\,\text{mm}$, and $t = 0.8\,\text{ns}$ above the radiating source.

along the y-axis in the vertical cut-plan equated by $x = 0\,\text{mm}$ was made. As a consequence, one gets the graphs displayed in Fig. 11.

These figures depict the comparison of the extracted E-field component profiles and those obtained from the exact calculations. Due to the numerical inaccuracies during the *fft* and *PWS*-transforms, one finds that slight level magnitude differences are found especially for E_y and E_z. Nonetheless, the level differences between the maximal values of the E-field, similar behaviour between the results yielded from the direct calculation and the proposed technique is found. Therefore, one finds that there is a good correlation between the direct calculation and the calculation from the proposed technique.

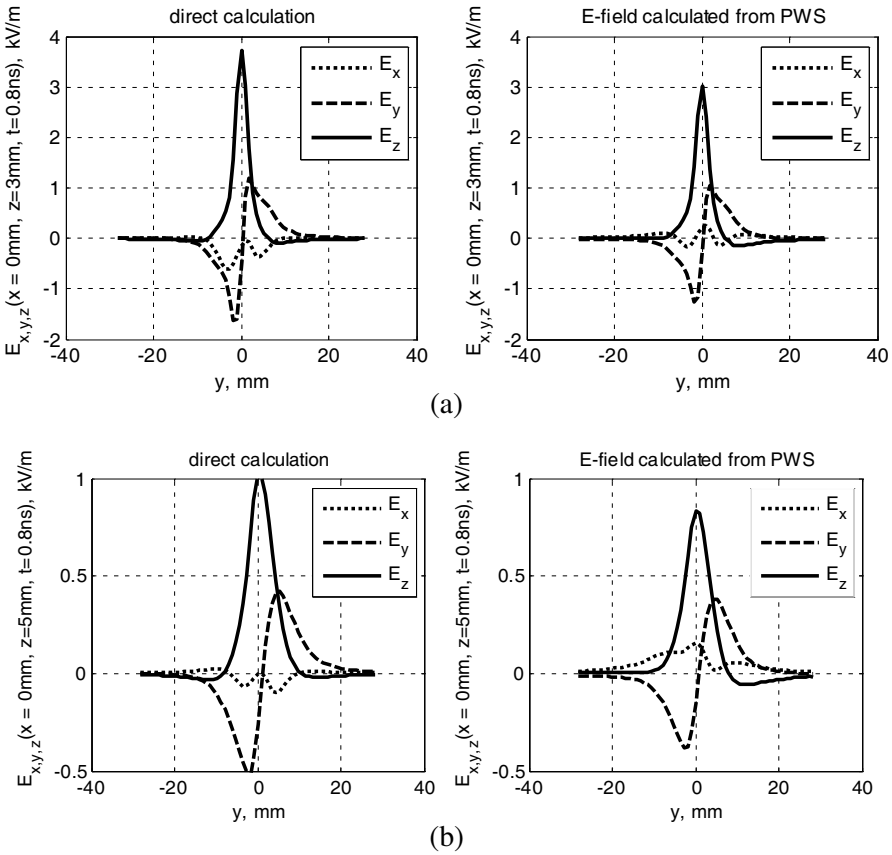

Figure 11. Profiles of the E-field components in the cut plan equated by $x = 0\,\text{mm}$ at (a) $z = 3\,\text{mm}$ and (b) $z = 5\,\text{mm}$, and $t = 0.8\,\text{ns}$ above the radiating source (direct calculation results in left and results from the proposed technique in right).

It is worth noting that very high space- and time-resolutions of the considered EM-field mapping plan are necessary to achieve more accurate results. Of course, the numerical computation of the here proposed calculation technique depends strongly on the performance of the used PC. For example, by using a PC equipped by Intel Core 2 Duo CPU, P-8400 @ 2.26 GHz with memory 2 Go RAM and assuming the 2-D data of each H-field component as a table with $N_x \times N_y = 171 \times 171$ points, one assesses the elapsed time during the Matlab computation of about 1754.77 seconds. The inaccuracies of the mappings presented are due to the numerical mathematical calculations as a whole, with their own limits and boundaries which depend on the used PC.

5. CONCLUSION

A time-domain innovative technique of the E-field extraction from the H-field mapped in near-zone of the radiating source by using the PWS method is reviewed. Originally, different from the classical computation methods in far-field, the introduced technique takes into account the influence of the evanescent EM-wave contribution.

The different steps of the proposed technique methodology were explained in detail. It was shown that from the time-dependent tensorial matrix data of the three H-field components $H_x(x, y, z, t)$, $H_y(x, y, z, t)$ and $H_z(x, y, z, t)$ given in the mapping plan positioned at the height $z = z_0$ above the radiating source (here assumed as a set of electric dipoles) should be transposed in the equivalent frequency-dependent data through the classical *fft*-operation. Then with the obtained results, one can determine the frequency-dependent tensorial matrix associated to E-field components $E_x(x, y, z_0, f)$, $E_y(x, y, z_0, f)$ and $E_z(x, y, z_0, f)$ by using the Maxwell-Ampere relation and PWS-transform [14–22]. In order to achieve the desired equivalent time-domain E-field components $E_x(x, y, z_0, t)$, $E_y(x, y, z_0, t)$ and $E_z(x, y, z_0, t)$, it is necessary to apply the *ifft*-operation. Thus the algorithm of the under study extraction technique was implemented into Matlab program. In order to evidence the feasibility of the proposed technique, one considers the EM-radiation of the combination of hertzian dipole elements excited by ultra-short duration transient pulse current [22–24]. One points out that the introduced computation method may be extrapolated to other radiating sources other than the five dipoles initially chosen. In order to take into account the evanescent EM-wave influence in near-field, one chooses the distances between the mapping plan and the considered radiating source z_0, below one-sixth of the minimal wavelength. As results of the computation, it was demonstrated that from the given H-field

component data calculated at the heights $z_0 = 3\,\text{mm}$ and $z_0 = 5\,\text{mm}$ above the radiating source formed by a set of dipoles placed in the plan equated by $z = 0$, one gets cartographies of E-field components having behaviours perfectly in good agreement with those obtained from the direct calculations with the analytical formulations. Most importantly, it was evidenced equally that the profiles of these E-field components present the same behaviours. Due to the numerical inaccuracy during the *fft*- and *PWS*-operations, one assesses relative errors lower than 10%. It is interesting to point out that compared to the finite-differences time domain (FDTD) method, this technique is advantageous on the computation time and its flexibility to the treatment of the measured EM-near-field data mapped in 2-D.

In the continuation to this work, one envisages to apply this EM-field calculation method for the determination of the E-field radiation cartography knowing the H-field in certain solvers which are able to compute only the H-field in the time domain as the case of the popular 3-D EM simulator Maxwell3D of Ansys$^{\text{TM}}$. In addition, the presented technique can be used also in the EMC applications related to the analysis of the transient E-field emissions as introduced in [8, 11, 12].

REFERENCES

1. Commens, M. and L. Murphy, "Full vehicle EMI/EMC studies," *Application Workshops for High-performance Electronic Design*, Minneapolis, MN, Feb. 2, 2007.
2. Hongmei, F., "Far field radiated emission prediction from magnetic near field magnitude-only measurements of PCBs by genetic algorithm," *IEEE EMC Symp.*, 321–324, Austin, Aug. 17–21, 2009.
3. Ansys, "Full system EMI/EMC methodology," ANSYS High-performance Electronics Seminars, Phoenix, Arizona, Jun. 10, 2010.
4. Malcovati, P. and F. Maloberti, "Integrated microsystem for 3D magnetic field measurements," *Aerospace and Electronic Systems Magazine*, Vol. 14, No. 9, 43–46, Sep. 1999.
5. Sonia, B. D., M. Ramdani, and E. Sicard, *Electromagnetic Compatibility of Integrated Circuits. Techniques for Low Emission and Susceptibility*, 464, Springer, New York, 2006.
6. Klotz, F., "EMC test specification for integrated circuits," *18th Int. Symp. EMC*, 73–78, Zurich, Sep. 24–28, 2007.
7. Song, Z., S. Donglin, F. Duval, A. Louis, and D. Fei, "A novel electromagnetic radiated emission source identification

methodology," *Asia-Pacific Symposium on EMC*, Pekin, China, Apr. 12–16, 2010.

8. Winter, W. and M. Herbrig, "Time domain measurement in automotive applications," *Proc of IEEE Int. Symp. EMC*, 109–115, Austin, Texas, USA, Aug. 17–21, 2009.
9. Essakhi, B., D. Baudry, O. Maurice, A. Louis, L. Pichon, and B. Mazari, "Characterization of radiated emissions from power electronic devices: Synthesis of an equivalent model from near-field measurement," *Eur. Phys. J. Appl. Phys.*, Vol. 38, 275–281, 2007.
10. Vives-Gilabert, Y., C. Arcambal, A. Louis, F. Daran, P. Eudeline, and B. Mazari, "Modeling magnetic radiations of electronic circuits using near-field scanning method," *IEEE Tran. EMC*, Vol. 49, No. 2, 391–400, 2007.
11. Rammal, R., M. Lalande, E. Martinod, N. Feix, M. Jouvet, J. Andrieu, and B. Jecko, "Far field reconstruction from transient near-field measurement using cylindrical modal development," *International Journal of Antennas and Propagation*, Vol. 2009, Article ID 798473, Hindawi, 2009.
12. Cicchetti, R., "Transient analysis of radiated field from electric dipoles and microstrip lines," *IEEE Trans. Ant. Prop.*, Vol. 39, No. 7, 910–918, Jul. 1991.
13. Ansys, "Thermal stress analysis on IGBT power system design," ANSYS High-performance Electronics Seminars, Phoenix, Arizona, Jun. 10, 2010.
14. Balanis, C. A., *Antenna Theory: Analysis and Design*, 3rd edition, Wiley, New York, 2005.
15. Paris, D. T., W. M. Leach, and E. B. Joy, "Basic theory of probe-compensated near-field measurements," *IEEE Tran. Ant. Prop.*, Vol. 26, No. 3, 373–379, May 1978.
16. Wang, J. J. H., "An examination of the theory and practices of planar near-field measurement," *IEEE Tran. Ant. Prop.*, Vol. 36, No. 6, 746–753, Jun. 1988.
17. Korpel, A., "Plane wave spectra," PDF electronic files, 13 pages, 1996, Available online: www.engineering.uiowa.edu/∼adriank/book/smroads/plane.pdf.
18. Masters, G. F., "Probe-correction coefficients derived from near-field measurements," *Ant. Measurement Techniques Association (AMTA) Symposium*, Oct. 7–11, 1991.
19. Shi, J., M. A. Cracraft, K. P. Slattery, M. Yamaguchi, and R. E. DuBroff, "Calibration and compensation of near-field scan

measurements," *IEEE Tran. EMC*, Vol. 47, No. 3, 642–650, Aug. 2005.

20. Cauterman, M., I. Seignolles, D. Lecointe, and J. C. Bolomey, "Plane waves spectrum in reverberating chambers," *Workshop on EMC Measurement Techniques for Complex and Distributed System*, Lille, France, Jun. 11–12, 2001.
21. Baudry, D., M. Kadi, C. Arcambal, Z. Riah, Y. Vives-Gilabert, A. Louis, and B. Mazari, "Plane wave spectrum theory applied to near-field measurements for EMC investigations," *Science, Measurement & Technology, IET*, Vol. 3, No. 1, 72–83, Jan. 2009.
22. Hertz, H. R., "Untersuchungen ueber die Ausbreitung der elektrischen Kraft," *Johann Ambrosius Barth*, Leipzig, 1892 (in German).
23. Schantz, H. G., "Electromagnetic energy around hertzian dipoles," *IEEE Tran. Ant. Prop. Magazine*, Vol. 43, No. 2, 50–62, Apr. 2001.
24. Sten, J. C.-E. and A. Hujanen, "Aspects on the phase delay and phase velocity in the electromagnetic near-field," *Progress In Electromagnetics Research*, Vol. 56, 67–80, 2006.